

Spectral Evolution of a New X-ray Transient MAXI J0556–332 Observed by MAXI, Swift, and RXTE

Mutsumi SUGIZAKI¹, Kazutaka YAMAOKA², Masaru MATSUOKA^{1,3}, Jamie A. KENNEA⁴, Tatehiro MIHARA¹, Kazuo HIRO⁵, Masaki ISHIKAWA⁶, Naoki ISOBE⁷, Nobuyuki KAWAI⁸, Masashi KIMURA⁹, Hiroki KITAYAMA⁹, Mitsuhiro KOHAMA³, Takanori MATSUMURA¹⁰, Mikio MORII⁸, Yujin E. NAKAGAWA¹¹, Satoshi NAKAHIRA¹, Motoki NAKAJIMA¹², Hitoshi NEGORO¹³, Motoko SERINO¹, Megumi SHIDATSU⁵, Tetsuya SOOTOME¹, Kousuke SUGIMORI⁸, Fumitoshi SUWA¹³, Takahiro TOIZUMI⁸, Hiroshi TOMIDA³, Yoko TSUBOI¹⁰, Hiroshi TSUNEMI⁹, Yoshihiro UEDA⁵, Shiro UENO⁵, Ryuichi USUI⁸, Takayuki YAMAMOTO¹, Makoto YAMAUCHI¹⁴, Kyohei YAMAZAKI¹⁰, Atsumasa YOSHIDA², and the MAXI team

¹MAXI team, Institute of Physical and Chemical Research (RIKEN), 2-1 Hirosawa, Wako, Saitama 351-0198
sugizaki@riken.jp

²Department of Physics and Mathematics, Aoyama Gakuin University, 5-10-1 Fuchinobe, Sagami-hara, Kanagawa 229-8558

³ISS Science Project Office, Institute of Space and Astronautical Science (ISAS), Japan Aerospace Exploration Agency (JAXA), 2-1-1 Sengen, Tsukuba, Ibaraki 305-8505

⁴Department of Astronomy and Astrophysics, 0525 Davey Laboratory, Pennsylvania State University, University Park, PA 16802, USA

⁵Department of Astronomy, Kyoto University, Oiwake-cho, Sakyo-ku, Kyoto 606-8502

⁶School of Physical Science, Space and Astronautical Science, The Graduate University for Advanced Studies (Sokendai), 3-1-1 Yoshinodai, Chuo-ku, Sagami-hara, Kanagawa 252-5210

⁷Institute of Space and Astronautical Science (ISAS), Japan Aerospace Exploration Agency (JAXA), 3-1-1 Yoshino-dai, Chuo-ku, Sagami-hara, Kanagawa 252-5210

⁸Department of Physics, Tokyo Institute of Technology, 2-12-1 Ookayama, Meguro-ku, Tokyo 152-8551

⁹Department of Earth and Space Science, Osaka University, 1-1 Machikaneyama, Toyonaka, Osaka 560-0043

¹⁰Department of Physics, Chuo University, 1-13-27 Kasuga, Bunkyo-ku, Tokyo 112-8551

¹¹Research Institute for Science and Engineering, Waseda University, 17 Kikui-cho, Shinjuku-ku, Tokyo 162-0044

¹²School of Dentistry at Matsudo, Nihon University, 2-870-1 Sakaecho-nishi, Matsudo, Chiba 101-8308

¹³Department of Physics, Nihon University, 1-8-14, Kanda-Surugadai, Chiyoda-ku, Tokyo 101-8308

¹⁴Department of Applied Physics, University of Miyazaki, 1-1 Gakuen Kibanadai-nishi, Miyazaki, Miyazaki 889-2192

(Received ; accepted)

Abstract

We report on the spectral evolution of a new X-ray transient, MAXI J0556–332, observed by MAXI, Swift, and RXTE. The source was discovered on 2011 January 11 (MJD=55572) by MAXI Gas Slit Camera all-sky survey at $(l, b) = (238^\circ.9, -25^\circ.2)$, relatively away from the Galactic plane. Swift/XRT follow-up observations identified it with a previously uncatalogued bright X-ray source and led to optical identification. For more than one year since its appearance, MAXI J0556–332 has been X-ray active, with a 2–10 keV intensity above 30 mCrab. The MAXI/GSC data revealed rapid X-ray brightening in the first five days, and a hard-to-soft transition in the meantime. For the following ~ 70 days, the 0.5–30 keV spectra, obtained by the Swift/XRT and the RXTE/PCA on an almost daily basis, show a gradual hardening, with large flux variability. These spectra are approximated by a cutoff power-law with a photon index of 0.4–1 and a high-energy exponential cutoff at 1.5–5 keV, throughout the initial 10 months where the spectral evolution is mainly represented by a change of the cutoff energy. To be more physical, the spectra are consistently explained by thermal emission from an accretion disk plus a Comptonized emission from a boundary layer around a neutron star. This supports the source identification as a neutron-star X-ray binary. The obtained spectral parameters agree with those of neutron-star X-ray binaries in the soft state, whose luminosity is higher than 1.8×10^{37} erg s^{−1}. This suggests a source distance of > 17 kpc.

Key words: X-rays: stars — X-rays: individual (MAXI J0556–332) — stars: neutron

1. Introduction

Galactic X-ray binaries distributed near the Galactic plane, exhibiting some of the brightest X-ray fluxes in the sky, have been well studied since the beginning of X-ray astronomy (e.g. Hayakawa 1981). Their X-ray emission is

thought to occur when the gas from a companion (often late type) star accretes onto a compact star, a neutron star (NS) or a black hole (BH). They often show a large degree of X-ray flux variability and long periods of quiescence, only appearing in single (or sometimes recurring) periods of transient X-ray activity. Many attempts have

been made to understand the behavior of these objects in a unified scheme, particularly employing accretion-disk theory (Shakura & Sunyaev 1973).

So far, the standard-disk picture has successfully explained the X-ray emission from NS binaries with weak magnetic fields in their bright phase (Mitsuda et al. 1984; Makishima et al. 1986). Our next task is to understand their variations, particularly spectral state transitions that are often seen when these sources exhibit transient outbursts. Although RXTE, INTEGRAL, and Swift survey observations with wide sky coverages provided useful information, few works have been done on the initial transitions. In particular, these studies on NS X-ray transients are limited because they are much fainter than BH X-ray novae.

The unbiased all-sky monitoring with Monitor of All X-ray Image (MAXI; Matsuoka et al. 2009) allows us to detect X-ray novae and transients, and to follow their intensity evolution from the beginning to the end. The MAXI mission started in 2009 August and has already detected several X-ray transients and novae in their initial phase (e.g. Nakahira et al. 2010; Yamaoka et al. 2011; MAXI web site¹). Asai et al. (2012) studied the initial rising behavior of outbursts from two transient NS low-mass X-ray binaries (LMXBs), Aql X-1 and 4U 1608-52, and then derived a relation between the initial hard-state duration and the hard-to-soft transition luminosity.

In the constellation Columba, a new X-ray transient, MAXI J0556–332, was discovered by the MAXI Gas Slit Camera (GSC; Mihara et al. 2011) at 9:21 (UT) on 2011 January 11 (Matsumura et al. 2011). Its position in Galactic coordinates, $(l, b) = (238^\circ.9, -25^\circ.1)$, is relatively away from the Galactic plane. A Swift (Gehrels et al. 2004) follow-up observation confirmed a bright uncatalogued X-ray source within the MAXI error circle and localized the source position at J2000 coordinates of $(\alpha, \delta) = (89^\circ.19300, -33^\circ.17451) = (5^h56^m46^s.32, -33^\circ10'28''.2)$ with the positional uncertainty of $1''.7$ (Kennea et al. 2011). The X-ray source agrees in position with an optical star with a B -magnitude of 19.4. RXTE Target-of-Opportunity (ToO) observations were also performed. The results revealed complex time variability, together with energy spectra that can be represented by a sum of a multi-color disk blackbody (diskBB in Xspec terminology) and a blackbody (BB) (Strohmayer & Smith 2011; Strohmayer 2011; Belloni et al. 2011). Based on color-color (CD) and hardness-intensity (HID) diagrams extracted from the RXTE data, Homan et al. (2011) suggested that the source is a transient neutron-star Z source. They estimated the source distance to be 20–35 kpc, from a change of the CD/HID tracks which is thought to occur at the same luminosity as in another transient Z source, XTE J1701–462 (e.g. Homan et al. 2010).

Follow-up observations of the optical counterpart found that the star had brightened to $R \sim 17.8$ from its USNO-B1.0 magnitude of $R = 19.9$, and the spectrum revealed emission lines indicating the presence of an accretion disk

around the compact accretor (Halpern 2011). It continued to brighten in the R -band until January 17, but slightly faded on January 18 (Russell et al. 2011). Optical spectroscopy revealed narrow emission lines in the Bowen blend, and a period search in radial velocities of these lines provided two candidate orbital periods, 16.43 ± 0.12 hrs and 9.754 ± 0.048 hrs (Cornelisse et al. 2011). A radio observation on January 19 with the Australia Telescope Compact Array detected a faint radio source (Coriat et al. 2011). Both the optical-to-X-ray and the radio-to-X-ray flux ratios suggest that the X-ray source is probably a NS binary rather than a BH binary, if it belongs to our Galaxy with a distance less than 20 kpc (Russell et al. 2011; Coriat et al. 2011). An XMM-Newton observation with the reflection grating spectrometer (RGS) detected a strong emission line near 24.8 \AA whose center energy is consistent with the $\text{Ly}\alpha$ transition of N VII in the rest frame. From an extremely high N/O line ratio revealed by this observation, the donor star is suggested to be a peculiar exotic star such as a hot subdwarf (sdB, sdO) or a white dwarf (Maitra et al. 2011).

These observational results suggest that MAXI J0556–332 is an X-ray binary, involving a collapsed object, located in the Galactic halo. The companion is not a regular late-type star, so that the source distance has not been determined better than the X-ray estimate of 20–35 kpc by Homan et al. (2011). Most of these results favor the collapsed component being a NS, although the BH scenario has not yet been completely ruled out.

This paper presents the X-ray behavior of MAXI J0556–332, including an initial transition and continuous long-term variations, observed by the MAXI GSC. We also analyzed spectral variations using data taken by the Swift/X-Ray Telescope (XRT; Burrows et al. 2005) and the RXTE/Proportional Counter Array (PCA; Jahoda et al. 2006) on an approximately daily cadence. We describe the observations and the data reduction in section 2, and present the analysis results in section 3. In section 4, the origin of the X-ray emission and its evolution are discussed. All the quoted errors are hereafter given at the 90% confidence limit, unless otherwise specified.

2. Observation and Data Reduction

2.1. MAXI/GSC

Every 92-minute orbital revolution, MAXI on the International Space Station (ISS) scans almost the whole sky with two kinds of X-ray cameras: the GSC working in the 2–30 keV energy band, and the Solid-state Slit Camera (SSC; Tsunemi et al. 2010; Tomida et al. 2011) in the 0.5–10 keV band. The new X-ray transient, MAXI J0556–332, first detected by the GSC on 2011 January 11, brightened to 80 mCrab in the 4–10 keV band within a day (Matsumura et al. 2011). The upper limit on the average 4–10 keV flux prior to the detection is $1.2 \text{ mCrab} = 1.5 \times 10^{-11} \text{ erg cm}^{-2} \text{ s}^{-1}$ (Hiroi et al. 2011). The source was also detected by the SSC when it was discovered by the GSC. However, the time coverage of the SSC was too limited to study spectral and flux changes. We therefore

¹ <http://maxi.riken.jp/top/>

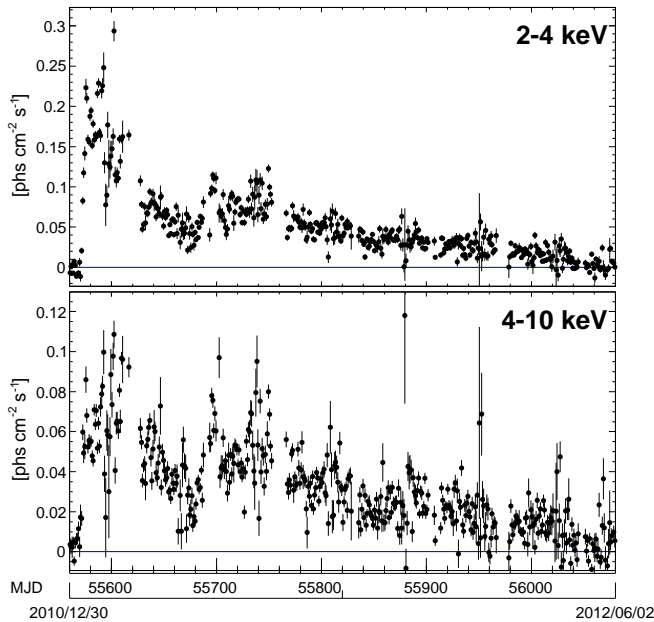


Fig. 1. MAXI/GSC light curves of MAXI J0556–332 in 2–4 keV (top) and 4–10 keV (bottom). Each data point represents a daily average.

concentrate on the GSC data.

Reduction and analysis of the GSC data were carried out following the standard procedure described by Sugizaki et al. (2011). The source event data were extracted from a rectangular area of $3^\circ.6$ along the detector anode wires and $3^\circ.0$ in the scan direction centered at the source position; the latter corresponds to the point spread function for each single scan transit of ~ 40 seconds. The background was collected from data taken in the same anode area just before and after each scan transit. With the same analysis procedure, we processed the light curve of the Crab nebula for the same period, and then confirmed that calibration uncertainties in the standard light curves in the 2–4 keV, 4–10 keV, and 10–20 keV energy bands are at most 5% at the $1\text{-}\sigma$ level.

Figure 1 shows the obtained GSC light curve of MAXI J0556–332 in the 2–4 keV and 4–10 keV bands for the entire 1.5-year active period. These data represent the unfolded photon flux per 1-day time bin. In the 10–20 keV band, the GSC did not detect any significant flux above $3\text{-}\sigma$ confidence limit, which is typically $0.015\text{ photons cm}^{-2}\text{ s}^{-1}$ (45 mCrab).

2.2. *Swift*/XRT

Swift/XRT pointing observations of MAXI J0556–332 were performed over 112 epochs until 2011 November 22 utilizing the Windowed Timing (WT) mode and a typical exposure of 0.5–1 ks. Using the archival Swift/XRT data, we investigated the evolution of the 0.3–10 keV energy spectrum. The data reduction and analysis were performed using the Swift analysis software version 3.8, released as a part of HEASOFT 6.11 and CALDB (calibration database) files of version 20110915, provided

via NASA/GSFC. Since the WT data are 1-dimensional, only spatial information in the CCD detector X (DETX) direction is available. The source events were collected from a 40 pixel wide region centered on the target position, and the backgrounds were collected from a region with the same width as the source region and 40-pixel away from the target along the DETX direction. In spectral model fitting, we used an XRT response matrix file, `swxwt0to2s6.20010101v014.rmf`, and ancillary response files built by `xrtmkarf`. A systematic error of 2% was implemented (Godet et al. 2009).

2.3. *RXTE*/PCA

From 2011 January 13 to 2011 December 29, MAXI J0556–332 was observed with RXTE/PCA on an almost daily basis with a typical exposure of 1–2 ks. The obtained data provides useful information in the energy range from 3 to 30 keV. We performed reduction of the PCA data with the standard RXTE analysis tools released as a part of HEASOFT 6.11 and the CALDB files of version 20111102 provided via NASA/GSFC. We used the PCA `standard-2` data with a time resolution of 16-s for the spectral analysis, and the `Good-Xenon` data with a time resolution of $1\text{-}\mu\text{s}$ for the light-curve analysis. All the data was screened with the standard selection criteria: the spacecraft pointing offset is smaller than $0^\circ.02$, the earth-limb elevation angle is larger than 10° , and the time since the last South Atlantic Anomaly passage is longer than 30 minutes. We used event data detected only on the top layer of the Proportional Counter Unit (PCU) #2, which is the best calibrated among all counter units. The background was estimated using the archived background model provided by the instrument team². The response matrix files were built with `pcarsp` for each pointing observation. A systematic error of 0.5% was applied.

3. Analysis and Results

3.1. Long-Term Light Curve and Color Variations

In order to investigate long-term flux and hardness variations with a good statistic accuracy, we first extracted five-band X-ray light curves from the Swift/XRT (0.3–6 keV) and RXTE/PCA (2–20 keV) data. Figure 2 shows the results from 2011 January 13 (MJD=55574) to 2011 December 29 (MJD=55924), together with soft-color (3.6–5.6 keV / 2.0–3.6 keV) and hard-color (8.5–18.4 keV / 5.6–8.5 keV) variations. In order to enable direct comparison among the different instruments, the observed count rates per 256-s time bin in each instrument were converted to the unfolded photon flux, assuming that the spectrum has a power-law with a photon index of 1 and a high-energy exponential cutoff at $E_{\text{cut}} = 3\text{ keV}$, with an interstellar absorption of $0.29 \times 10^{21}\text{ cm}^{-2}$; these are based on the spectral analysis in section 3.5. The Swift/XRT and RXTE/PCA data in the same energy band, taken within about a day, thus mostly agree with each other, which confirms general consistency between the two in-

² http://heasarc.gsfc.nasa.gov/docs/xte/pca_news.html

struments. The large flux discrepancy seen for a few data points close in time is indicative of flux changes between the pair of observations, which were not exactly simultaneous.

These light curves show complex energy-dependent variations, particularly during the initial ~ 50 days. In the lowest energy band (0.3–2 keV), the flux reached the maximum within a few days after the source emergence, and then decayed in about 50 days. In the highest energy band (8.5–18.4 keV), the flux in contrast increased gradually, reaching the maximum with large short-time variability on about the 50th day. The contrast between the soft and hard flux evolutions are clearly reflected in the soft-color and hard-color variations, because both colors largely increased during the initial 50 days.

As shown in figure 2, we divided the entire observation period into six intervals, A, B, C, D, E, and F; they are characterized as follows. Int-A: initial (30 days) phase when the intensity below 2 keV was highest and the hardest-band intensity increased gradually. Int-B: brightest phase in the 5.6–8.5 keV and harder bands, with large variability in the whole band. Int-C: decaying phase where the large variability in the 5.6–8.5 keV and harder bands still remains. Int-D: intermission phase where the average flux is lower than in the intervals just before and after. Int-E: re-brightening phase in the whole band with moderate variability. Int-F: low activity phase with a similar average flux to Int-D.

To better grasp the spectral changes associated with the intensity variations, we plot several CDs in figure 3, representing the correlation between the two colors extracted from the RXTE-PCA data. There, data from the six intervals defined in figure 2 are shown separately. All the six CDs apparently exhibit Z-like shapes as often observed in bright NS LMXBs (e.g. van der Klis 2006). This strongly supports the source identification as a NS X-ray binary. These CDs are also classified into two groups. The Int-C behavior resembles that of Int-E, while Int-D resembles Int-F. This agrees with the report by Homan et al. (2011) on this source, that the CD track changed between 2011 February (MJD \sim 55600) and 2011 September (MJD \sim 55800). According to two subgroups of the Z-like CDs, represented by Cyg X-2 and Sco X-1 (e.g. Homan et al. 2010), the CDs of Int-A, B, C, and E are classified into the Cyg X-2 group, while those of Int-D and F are into the Sco X-1 group.

In figure 4, we plot the two colors against the intensity, to create two HIDs. There, the six intervals are specified with the same color scheme as in figure 3. As Homan et al. (2011) reported, The change of the HID tracks among the six intervals is also clearly seen.

3.2. Color-Color and Hardness-Intensity Diagrams

3.3. Search for X-ray Burst Activity

From multi-wavelength observations reported so far (section 1) and the results of data analysis presented above, MAXI J0556–332 is considered most likely to be a NS X-ray binary. Transient NS X-ray binaries sometimes

emit type-I X-ray bursts, characterized by a fast rise in a few seconds and an exponential decay in a few tens of seconds (e.g. Lewin et al. 1993). Therefore, we searched the entire RXTE/PCA light curves for type-I X-ray bursts using 1-s time bins. However, we did not find any burst-like event with a count-rate increase higher than $50 \text{ c s}^{-1} \text{ PCU}^{-1}$ in the 2–20 keV band.

Even if the source is located at the distance of 35 kpc, which is the farthest limit estimated by Homan et al. (2011), we would have detected $\sim 98 \text{ c s}^{-1}$ with the RXTE/PCA from a typical X-ray burst, assuming a blackbody spectrum with a temperature of 2.1 keV and a luminosity as high as the Eddington luminosity of $2 \times 10^{38} \text{ erg s}^{-1}$ as seen in the typical type-I burst. Such a burst should have been observed with the RXTE/PCA.

3.4. Initial Transition Behavior

The initial emergent phase for about three days of MAXI J0556–332 was covered only by the MAXI/GSC all-sky survey. To clarify the source behavior meanwhile, we extracted 2–4 keV and 4–10 keV lightcurves in a 12-h time bin, and present them in figure 5. Like in figure 2, the GSC count rates were converted to the incident photon fluxes, to make the results approximately free from the instrumental responses. There, the Swift/XRT and the RXTE/PCA data are superposed, together with the hardness ratio and the 2–10 keV flux. The Swift/XRT and RXTE/PCA data points, each covering typically 0.5–2 ks (plotted with a bin width of 256 s), are significantly more scattered than the 12-h averaged GSC data, presumably due to short-term (e.g. $< 1 \text{ h}$) variations. However, the hardness ratios are always consistent among the three missions. This implies that the spectral shape did not change largely on a time scale of a day or shorter, at least in the initial phase.

The MAXI/GSC hardness ratio clearly shows a step-like decrease at MJD=55574.0 before the RXTE and Swift observations started. Therefore, the source is considered to have made a hard-to-soft transition at this epoch, when the flux was still rising rapidly. The flux then peaked at MJD=55575.5 in the presumable soft state.

3.5. X-ray Spectral Evolution

We carried out X-ray spectral analysis over the 0.5–30 keV broad band, by combining the Swift/XRT and RXTE/PCA data which are averaged over each observation (0.5–2 ks typically). Although these Swift and RXTE observations were not exactly simultaneous, any spectral change within a day is considered small as already noticed in section 3.1. We thus selected pairs of Swift and RXTE observations carried out within 12 hours, and performed their simultaneous fits. To avoid possible inconsistency between the two instruments, we left the PCA versus XRT normalization, $f_{\text{PCA/XRT}}$, free, and discarded those pairs of which the value of $f_{\text{PCA/XRT}}$ is deviated from the average ($= 1.12$) by more than 30%. The logs of the selected observations, totaling 72 pairs, are summarized in table 1. All spectral fitting was carried out using Xspec version 12.7.0, released as a part of HEASOFT 6.11.

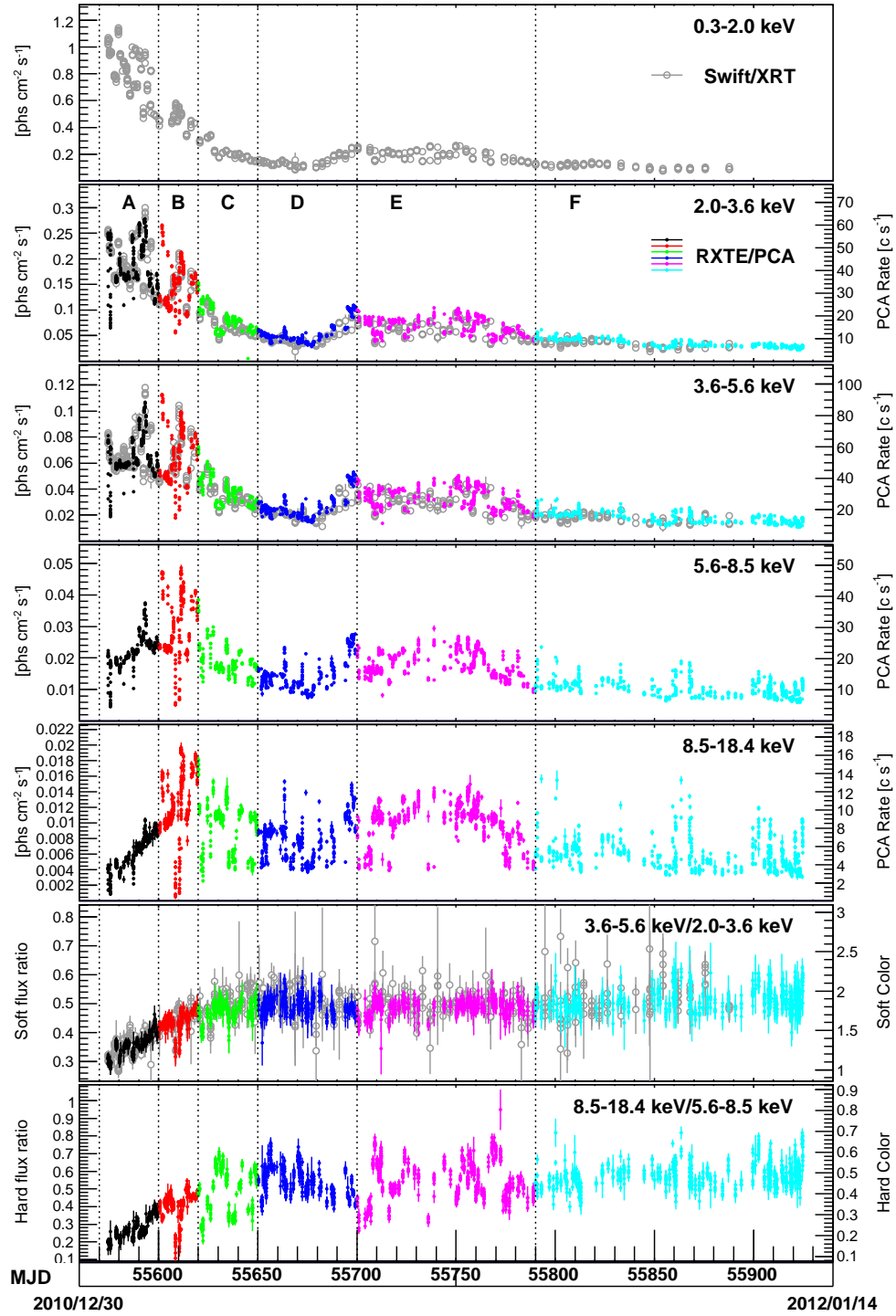


Fig. 2. Light curves in 0.3–2.0 keV, 2.0–3.6 keV, 3.6–5.6 keV, 5.6–8.5 keV, and 8.5–18.4 keV energy bands obtained by the Swift/XRT (gray) and the RXTE/PCA. Black, red, green, blue, purple and cyan specify intervals A, B, C, D, E, and F respectively, as labeled in the second panel. Soft color (3.5–5.6 keV / 2.0–3.6 keV) and hard color (8.5–18.4 keV / 5.6–8.5 keV) of the RXTE/PCA data are shown in the bottom two panels. All panels utilize 256-s time bin. All the vertical error bars represent the 1- σ statistical uncertainty.

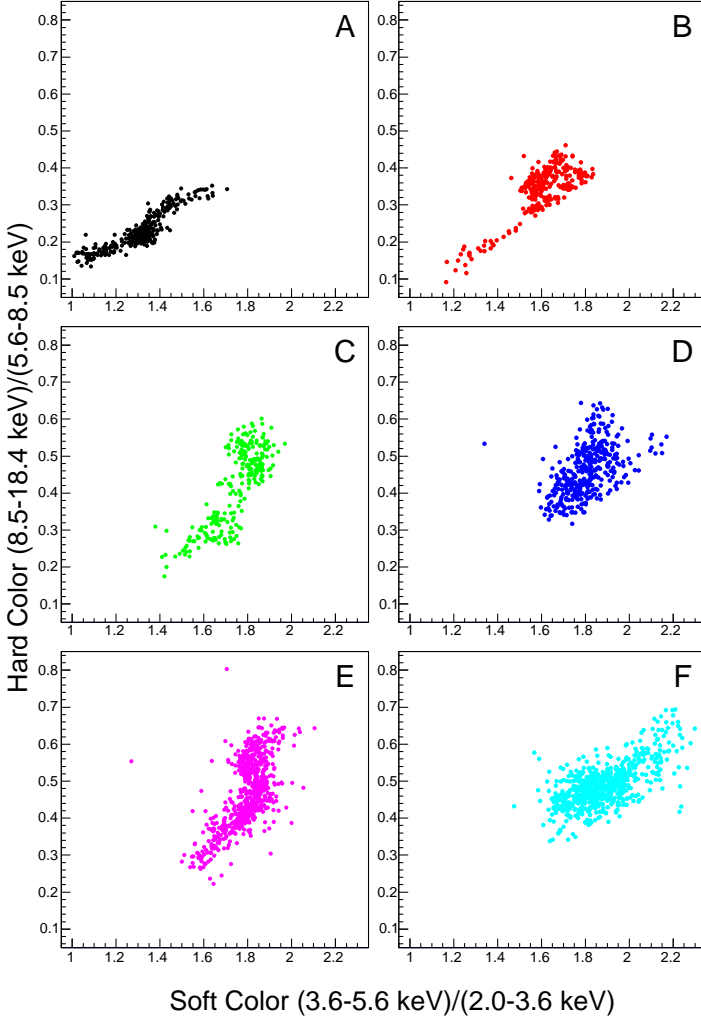


Fig. 3. Color-color diagrams (CDs) extracted from the RXTE-PCA data, for individual intervals of A, B, C, D, E, and F defined in figure 2.

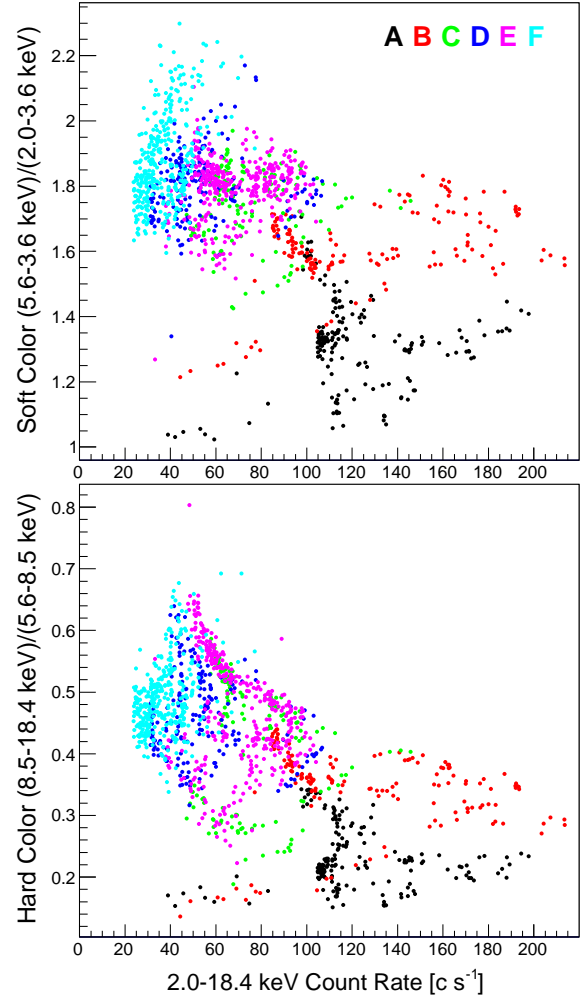


Fig. 4. Soft-color versus intensity (top) and hard-color versus intensity (bottom) diagrams extracted from the RXTE-PCA data. Data intervals of A, B, C, D, E, and F are colored similarly as in figure 2 and figure 3.

Figure 6 shows the XRT and PCA spectra in their unfolded $\nu f\nu$ form, from six typical observations, as indicated with arrows in the top panel of figure 7a. Including the six representatives, all the obtained spectra were found to show a featureless continuum, without any significant emission or absorption features. We first attempted to fit them with a simple continuum model of either a power law (PL), a blackbody (BB), a broken power-law (`bknpower`), or a power law with a high-energy exponential cutoff (`cutoffpl`), all multiplied with photoelectric absorption (`wabs`, Morrison & McCammon 1983) with free column density N_{H} . Then, 50 out of the 72 spectral pairs were reproduced by the `wabs*cutoffpl` model with reduced chi-squared (χ^2_{ν}) within the 99% confidence limits, while none of the other models were as successful on any data set. Figure 7a plots time evolution of best-fit `wabs*cutoffpl` model parameters, together with absorption-corrected 0.1–100 keV fluxes. Thus, the photon index Γ was in the range of 0.4–1 throughout, while

the cutoff energy E_{cut} changed from ~ 1.5 keV to ~ 5 keV. The flux decreased from 4×10^{-9} to 5×10^{-10} erg $\text{cm}^{-2} \text{s}^{-1}$ over the 10 months in agreement with the light curve (figure 2). The best-fit parameters for the spectra in figure 6 are summarized in table 2.

The spectrum, represented by a cutoff power-law with $\Gamma = 0.4\text{--}1$ and $E_{\text{cut}} = 1.5\text{--}5$ keV, roughly agrees with those of typical bright NS-LMXBs. The cutoff energy could represent the temperature of blackbody radiation from a neutron-star surface (e.g. Mitsuda et al. 1984, Mitsuda et al. 1989). We thus attempted a canonical two-component model for bright NS-LMXBs, consisting of a multi-color-disk blackbody (`diskBB` in Xspec terminology) and a blackbody (BB) (Mitsuda et al. 1984). However, as shown in figure 7a (fifth panel) and table 2, the best-fit χ^2_{ν} values of the `wabs*(diskBB+BB)` fits were no better than those with the `wabs*cutoffpl`. The residuals revealed excess features at both low and high energies, which can be considered as a signature of a

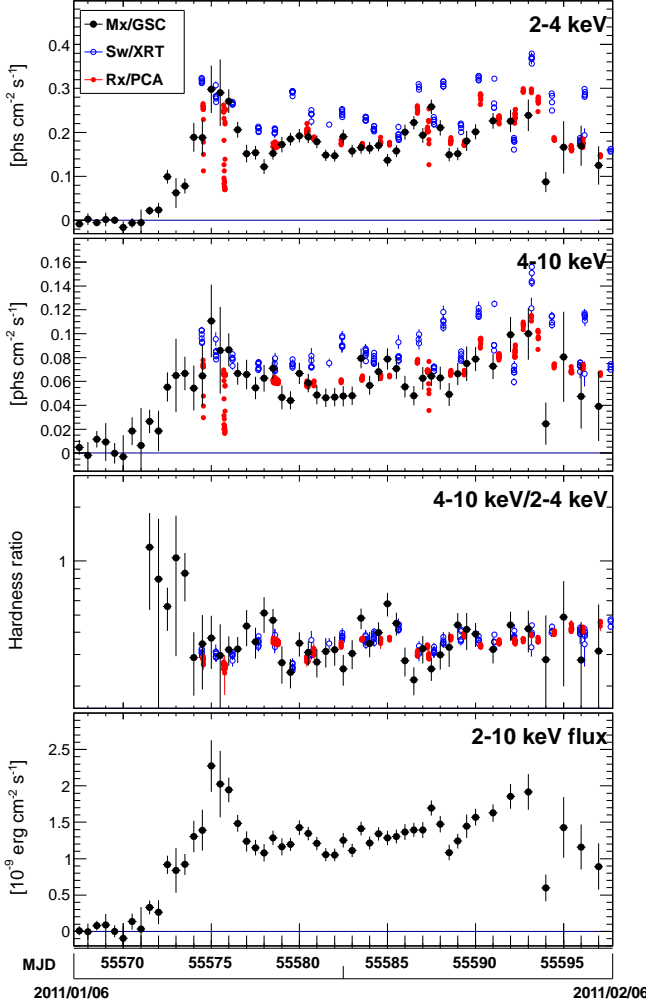


Fig. 5. Two-band MAXI/GSC light curves (black) during the initial phase, plotted since five days before the first detection. Each data point is an average over 12 hours. The Swift/XRT and RXTE/PCA data in 256-s time bin are overlaid in blue and red, respectively. Hardness ratio (4–10 keV / 2–4 keV) and the 2–10 keV flux are shown in the third and the fourth panels, respectively.

Comptonization process. Following Lin et al. (2007) and Lin et al. (2009), we hence tried to add a broken power-law function approximating the Comptonized component to the canonical two-component model, but the model `wabs*(diskBB+BB+bknpower)` did not improve the fit significantly.

We then examined more rigorously the Comptonization emission process, employing a thermally Comptonized continuum model, `nthcomp` in Xspec terminology (Zdziarski et al. 1996; Życki et al. 1999). It describes Comptonized emission arising when thermal seed photons with a BB or a `diskBB` spectrum is up-scattered by a hot thermal electrons with a temperature kT_e . This model uses an asymptotic power-law photon index Γ , which is related with kT_e and the scattering optical depth τ as

$$\Gamma = \left[\frac{9}{4} + \frac{1}{\frac{kT_e}{m_e c^2} \tau \left(1 + \frac{\tau}{3}\right)} \right]^{\frac{1}{2}} - \frac{1}{2} \quad (1)$$

(Sunyaev & Titarchuk 1980).

The `nthcomp` model alone, with seed photons of neither BB nor `diskBB`, was able to fit the observed spectra, even if the N_H was left free. The residuals showed a large discrepancy in the soft X-ray band below 2 keV. Adding another soft thermal component, of which the spectral shape is the same as that of the seed photons, did not improve the fit. However, when the temperature of the soft component was allowed to be free, and hence is different from the seed-photon temperature, the Comptonization plus soft-component model became acceptable. Therefore, the seed photons for Comptonization and the additional soft component must be of different origin.

When the additional soft component is represented by a BB model, the fit always made the absorption column density $N_H < 0.1 \times 10^{21} \text{ cm}^{-2}$. This upper limit is significantly lower than the Galactic H_I density of $0.29 \times 10^{21} \text{ cm}^{-2}$ in the source direction (Kalberla et al. 2005). This would contradict the high Galactic latitude ($|b| = 25^\circ 2$) and the suggested large distance, which place MAXI J0556–332 well outside the Galactic disk. On the other hand, an alternative model employing a `diskBB` for the soft component always gave the best-fit N_H which is larger than the Galactic H_I . Therefore, we hereafter use the `diskBB` model for the soft component.

Then, how about the seed-photon spectrum? If the optical depth of the Comptonizing medium is high enough ($\tau \gg 1$), whether the seed photon spectrum follows a BB or a `diskBB` model causes little difference in the emergent spectrum, and therefore are difficult to distinguish. Hence, we assume that the seed photons have a BB spectrum. In section 4.2, We discuss the validity of this model from the obtained best-fit parameters.

Using the `wabs*(diskBB+nthcomp)` model with a BB seed-photon source, we fitted all the spectrum pairs, and obtained successful fits as exemplified in figure 6. Then, assuming that the Comptonization process conserves the photon number in the original BB radiation, we estimated the radius of the BB seed-photon sphere R_{seed} according to the formula of

$$\begin{aligned} & F_{\text{nthcomp}}(T_{\text{seed}}, R_{\text{seed}}, d) \quad (\text{photons cm}^{-2} \text{ s}^{-1}) \\ &= \int f_{\text{BB}}(E, T_{\text{seed}}, R_{\text{seed}}, d) dE \\ &= 20.1 \left(\frac{kT_{\text{seed}}}{1 \text{ keV}} \right)^3 \left(\frac{R_{\text{seed}}}{1 \text{ km}} \right)^2 \left(\frac{d}{10 \text{ kpc}} \right)^{-2}, \end{aligned} \quad (2)$$

where $F_{\text{nthcomp}}(T_{\text{seed}}, R_{\text{seed}}, d)$ is the incident photon flux calculated from the best-fit model parameters in Xspec, T_{seed} is the seed-photon BB temperature, d is the source distance, and $f_{\text{BB}}(E, T_{\text{seed}}, R_{\text{seed}}, d)$ is the photon-flux spectrum of a BB emission. Including the values of R_{seed} , the best-fit model parameters from the six representative spectra are given in table 2.

Figures 7b show temporal variations of the best-fit parameters, including τ and R_{seed} derived using equations

Table 1. List of Swift/XRT and RXTE/PCA observation pairs used in the simultaneous spectral fits

MJD	Swift/XRT					RXTE/PCA				
	Obs ID	Date [†]	Start	End	Exp.[s]	Obs ID	Date [†]	Start	End	Exp.[s]
55574*	00031914001	01/13	10:51	11:14	1413	96371-01-02-00	01/13	12:32	13:22	2912
55575	00031914002	01/14	06:10	06:31	1277	96371-01-01-00	01/14	16:44	19:06	5936
55578	00031914005	01/17	14:23	14:42	1125	96371-01-03-00	01/17	12:13	19:24	15872
55580	00031914007	01/19	16:09	16:24	891	96371-01-04-01	01/19	19:35	20:00	864
55582	00031914009	01/21	10:10	10:33	1375	96371-01-05-00	01/21	08:52	09:17	1456
55583*	00031914010	01/22	18:15	18:39	1466	96371-01-05-01	01/22	13:02	13:51	2800
55584	00031914011	01/23	05:30	05:54	1480	96371-01-05-02	01/23	14:27	14:57	1616
55587	00031914014	01/26	15:13	15:37	1442	96371-01-05-05	01/26	08:06	08:48	2352
55588	00031914015	01/27	04:03	04:19	955	96371-01-05-06	01/27	13:56	14:36	2224
55589	00031914016	01/28	04:08	04:27	1167	96414-01-01-00	01/28	08:29	09:25	3200
55590	00031914017	01/29	04:13	04:28	938	96414-01-01-01	01/29	06:33	07:22	2752
55591	00031914018	01/30	01:21	01:38	1006	96414-01-01-02	01/30	07:30	08:27	3200
55593	00031914020	02/01	04:28	04:44	981	96414-01-01-07	02/01	04:05	04:21	800
55594	00031914021	02/02	08:01	08:16	900	96414-01-01-05	02/02	11:09	11:43	1872
55596	00031914023	02/04	04:48	05:07	1180	96414-01-02-00	02/04	02:33	02:54	1152
55597	00031914024	02/05	16:04	16:17	760	96414-01-02-07	02/05	23:26	23:39	768
55598	00031914025	02/06	19:30	19:34	252	96414-01-02-09	02/06	21:57	22:21	416
55600*	00031914027	02/08	10:10	10:30	1165	96414-01-02-04	02/08	11:10	11:59	2368
55606	00031914033	02/14	13:55	14:09	873	96414-01-03-03	02/14	13:03	15:00	2848
55607	00031914034	02/15	13:49	14:08	1147	96414-01-03-04	02/15	10:54	12:53	3408
55608	00031914035	02/16	13:52	14:08	959	96414-01-03-05	02/16	10:23	11:24	2896
55609	00031914036	02/17	12:32	12:52	1208	96414-01-03-06	02/17	16:23	16:43	336
55611	00031914038	02/19	07:43	08:05	1275	96414-01-04-01	02/19	05:48	09:52	8912
55614	00031914039	02/22	01:35	01:54	1144	96414-01-04-04	02/22	07:34	10:51	6144
55616	00031914040	02/24	04:58	05:18	1243	96414-01-04-06	02/24	11:19	11:40	880
55618	00031914041	02/26	02:06	02:13	441	96414-01-05-01	02/26	11:57	13:26	3040
55620*	00031914042	02/28	18:08	18:29	1260	96414-01-05-03	02/28	11:25	11:59	1872
55624	00031914044	03/04	17:07	17:30	1373	96414-01-06-00	03/04	12:14	12:48	2000
55626	00031914045	03/06	04:18	04:40	1309	96414-01-06-02	03/06	05:06	05:37	1872
55628	00031914046	03/08	02:46	03:09	1398	96414-01-06-04	03/08	13:25	14:22	3184
55630	00031914047	03/10	09:43	09:59	994	96414-01-06-06	03/10	09:28	09:49	1232
55632	00031914048	03/12	04:40	04:49	538	96414-01-07-01	03/12	11:31	12:21	2944
55634	00031914049	03/14	01:42	02:01	1148	96414-01-07-02	03/14	02:41	03:13	1888
55638	00031914051	03/18	13:21	13:40	1165	96414-01-08-00	03/18	12:02	12:35	1952
55640*	00031914052	03/20	15:12	15:32	1216	96414-01-08-02	03/20	10:59	11:20	1216
55642	00031914053	03/22	02:30	02:46	968	96414-01-08-04	03/22	01:09	01:19	608
55646	00031914055	03/26	10:45	11:04	1145	96414-01-09-00	03/26	07:55	08:47	2416
55648	00031914056	03/28	12:30	12:46	972	96414-01-09-03	03/28	08:36	09:19	2128
55650	00031914057	03/30	17:37	17:53	978	96414-01-09-05	03/30	10:52	11:10	592
55652	00031914058	04/01	19:13	19:34	1277	96414-01-10-01	04/02	06:04	08:33	5216
55654	00031914059	04/03	14:39	14:57	1092	96414-01-10-02	04/03	07:11	08:05	2592
55656	00031914060	04/05	21:14	21:33	1169	96414-01-10-05	04/06	02:53	03:26	2016
55658	00031914061	04/07	03:44	04:03	1156	96414-01-10-06	04/07	05:08	05:23	464
55662*	00031914063	04/11	05:50	06:11	1258	96414-01-11-02	04/11	14:21	15:14	2272
55664	00031914064	04/13	01:06	01:25	1143	96414-01-11-04	04/13	00:46	01:26	2320
55666	00031914065	04/15	01:19	01:42	1392	96414-01-12-00	04/15	12:21	12:43	1072
55670	00031914067	04/19	03:25	03:47	1340	96414-01-12-02	04/19	02:50	03:15	1488
55684	00031914071	05/04	02:48	03:03	874	96414-01-14-02	05/03	20:49	21:11	1328
55688	00031914072	05/07	11:16	11:33	1052	96414-01-15-01	05/07	07:51	08:48	3168
55694	00031914074	05/13	03:29	03:48	1183	96414-01-16-00	05/13	06:42	07:25	1904
55697	00031914075	05/16	10:20	10:39	1110	96414-01-16-03	05/16	06:50	07:24	1696
55700	00031914076	05/19	10:34	10:58	1479	96414-01-16-06	05/19	05:15	05:36	832
55706	00031914078	05/25	12:36	12:57	1245	96414-01-17-03	05/25	03:46	04:42	2688
55709	00031914079	05/28	01:35	01:56	1220	96414-01-18-01	05/28	02:12	03:13	3152
55712	00031914080	05/31	22:48	23:05	1055	96414-01-18-05	05/31	21:33	21:54	1280
55715	00031914081	06/03	19:57	20:15	1101	96414-01-19-00	06/04	03:57	04:33	2160
55718	00031914082	06/06	00:50	01:07	1059	96414-01-19-01	06/06	02:37	03:30	3088
55721	00031914083	06/09	01:05	01:27	1322	96414-01-19-03	06/09	02:43	04:15	3120
55724	00031914084	06/12	01:21	01:44	1377	96414-01-20-01	06/12	02:48	03:42	3184
55746	00031914091	07/04	16:06	16:29	1330	96414-01-23-01	07/05	02:32	02:56	1024
55749	00031914092	07/07	19:28	19:43	922	96414-01-24-00	07/08	00:57	02:56	3120
55752	00031914093	07/10	00:35	00:36	66	96414-01-24-02	07/10	03:12	03:34	864
55758	00031914095	07/16	12:02	12:18	974	96414-01-25-00	07/16	21:54	00:30	6288
55774	00031914099	08/01	10:35	10:51	997	96414-01-27-04	08/01	21:57	00:26	6032
55778	00031914100	08/05	18:34	18:49	948	96414-01-28-00	08/05	13:46	13:59	800
55782	00031914101	08/09	22:04	22:21	974	96414-01-28-04	08/09	18:12	18:33	1280
55785	00031914102	08/13	06:38	06:55	1021	96414-01-29-00	08/12	23:24	23:39	720
55790	00031914103	08/17	00:13	00:29	943	96414-01-29-03	08/17	03:22	03:43	784
55805	00031914107	09/02	03:13	05:01	6463	96414-01-31-05	09/01	20:35	21:16	2096
55809	00031914108	09/06	00:20	08:36	29714	96414-01-32-01	09/05	19:03	19:27	1472
55826	00031914112	09/22	06:40	06:57	974	96414-01-34-02	09/22	15:05	15:22	1024
55832	00031914113	09/29	05:46	05:57	678	96414-01-35-02	09/28	23:07	23:40	1792

*: Energy spectra are shown in figure 6 and the best-fit parameters are summarized table 2.

†: Date and time are in UT (Universal Time).

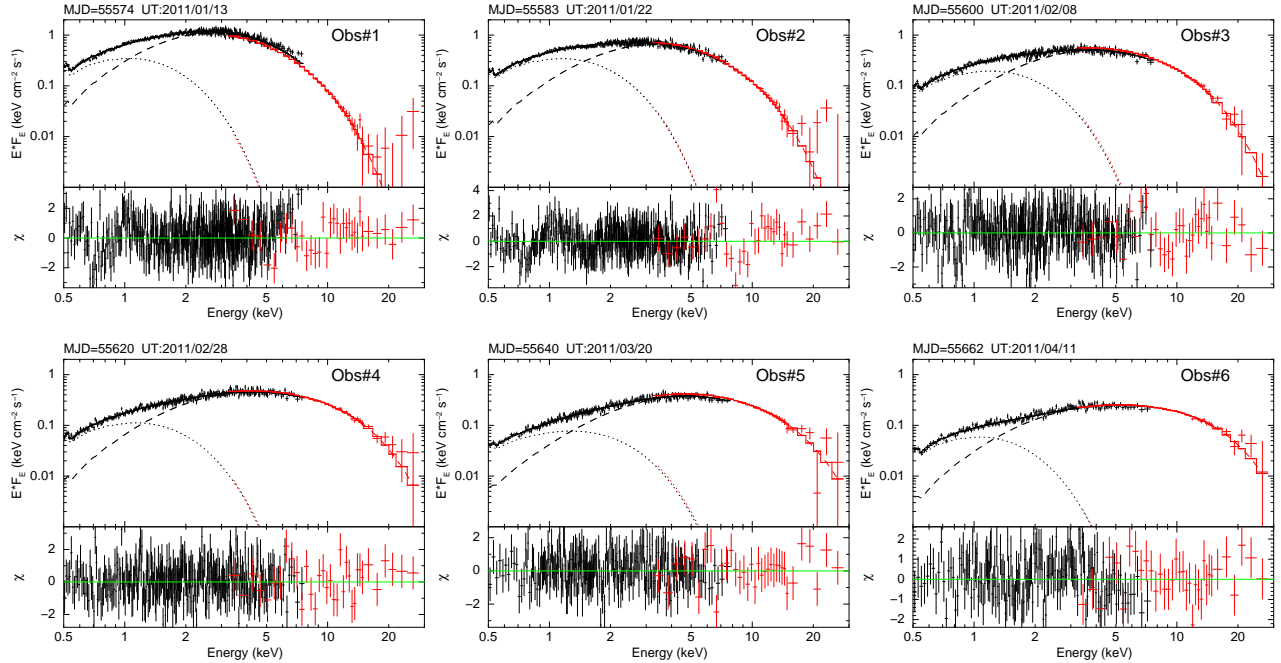


Fig. 6. Examples of unfolded $\nu f\nu$ spectra of MAXI J0556–332 obtained by the Swift/XRT (black) and the RXTE/PCA (red). The best-fit `wabs*(diskBB+nthcomp)` model and its residuals are shown together. The model parameters are summarized in table 2. Epochs of these six observations are indicated in the top panel of figures 7a.

(1) and (2) respectively, and the unabsorbed fluxes of the `diskBB` and `nthcomp` components. The values of R_{seed} and the `diskBB`-model parameter, $R_{\text{in}}/\sqrt{\cos i}$, related to the disk inner radius R_{in} and the inclination i , are calculated assuming $d = 10$ kpc. The actual radii are proportional to the source distance.

4. Discussion

MAXI J0556–332 is a new X-ray transient which appeared on 2011 January 11. Using the MAXI/GSC, Swift/XRT, and RXTE/PCA data, we studied the intensity and spectral evolution of this source over the entire active period for more than one year.

4.1. Source Identification from X-ray Spectrum

The wide-band (0.5–30 keV) X-ray spectra obtained by the Swift/XRT and XTE/PCA are featureless, and can be approximated by a cutoff power-law with $\Gamma \approx 0.4 - 1$ and $E_{\text{cut}} \approx 1.5 - 5$ keV. They are better fitted with a two-component model that consists of a multi-color-disk blackbody and a thermally Comptonized blackbody. This spectral model has often been used to describe X-ray emission from LMXBs containing a weakly-magnetized NS (e.g. Gierliński & Done 2002b; Sakurai et al. 2012) or a BH candidate (e.g. Done et al. 2004).

NS LMXBs have been largely classified into “Z-type” and “atoll-type” sources according to their CD-track shapes (Hasinger & van der Klis 1989; van der Klis 2006). The former objects are persistently as bright as L_{EDD} , and sometimes show rapid flux variations up to a factor of ~ 5 . The latter are fainter than the former, and of-

ten appear as transients or recurrent. The luminosity of atoll sources varies over a large range from $\sim 10^{-3}$ to ~ 0.2 times L_{EDD} , accompanied by spectral state changes. The higher-energy cutoff of 1.5–5 keV of MAXI J0556–332, represented by E_{cut} in the `wabs*cutoffpl` model or kT_e in the `wabs*(diskBB+nthcomp)` model, agrees well with those of the Z sources such as Cyg X-2 (Di Salvo et al. 2002), Sco X-1 (D’Aí et al. 2007), GX 5–1 (Sriram et al. 2011), GX 17+2 (Farinelli et al. 2005), and GX 349+2 (Di Salvo et al. 2001), whose luminosities are always $> 0.5 L_{\text{EDD}}$. The E_{cut} values of atoll sources are also below 5 keV in the soft state with the luminosity higher than $0.1 L_{\text{EDD}}$, while they tend to increase up to > 15 keV in the hard state with the luminosity of the order of $0.01 L_{\text{EDD}}$; the latter examples include Aql X-1 (Lin et al. 2007; Sakurai et al. 2012), 4U 0614+09 (Singh & Apparao 1994), 4U 1608–52 (Gierliński & Done 2002b; Lin et al. 2007; Takahashi et al. 2011), 4U 1705–44 (Barret & Olive 2002; Lin et al. 2010), and 4U 1728–34 (Tarana et al. 2011). Therefore, if the source is a NS LMXB, the X-ray luminosity should be higher than $0.1 L_{\text{EDD}} = 1.8 \times 10^{37}$ erg s $^{-1}$ in the observed period. The absorption-corrected model flux, which changed from 4×10^{-9} to 5×10^{-10} erg cm $^{-2}$ s $^{-1}$, constrains the source distance to be $d > 17$ kpc, in agreement with the estimate of $d = 20\text{--}35$ kpc by Homan et al. (2011) deduced from the luminosity at a CD-track transition.

Galactic BH X-ray binaries have been observed mostly in either of the two major spectral states, the low/hard or the high/soft state. These spectra are represented by a combination of thermal emission from the accretion disk and a Comptonized harder component (although de-

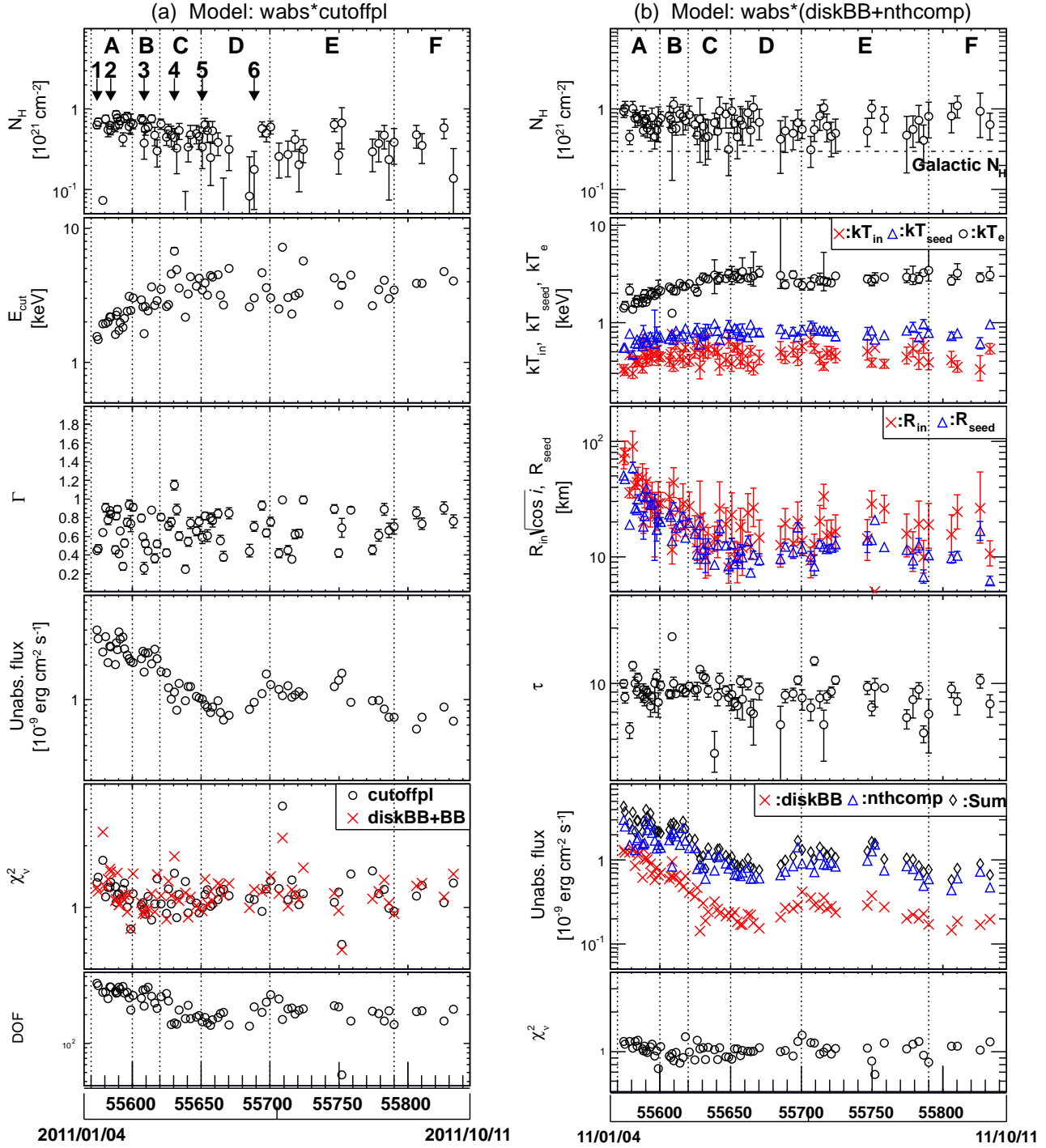


Fig. 7. Evolution of the best-fit spectral parameters, jointly determined with the Swift/XRT and the RXTE/PCA data. (a) The results from the empirical $\text{wabs}*\text{cutoffpl}$ fits. From top to bottom, the absorbing column density, the cutoff energy, the power-law index, the absorption-corrected model flux, the χ^2_{ν} values, and the degree of freedom. In the fifth panel, the fit goodness with an alternative $\text{wabs}*(\text{diskBB}+\text{BB})$ is shown in (red) cross. (b) The case with the more physical $\text{wabs}*(\text{diskBB}+\text{nthcomp})$ fits. In the third panel, R_{seed} and $R_{\text{in}}\sqrt{\cos i}$ are calculated in the assumed source distance of 10 kpc.

Table 2. Best-fit model parameters of six sample epochs obtained by Swift/XRT and RXTE/PCA combined spectral analysis

Observation-log Summary						
	Obs#1	Obs#2	Obs#3	Obs#4	Obs#5	Obs#6
Date(UT)	2011-01-13	2011-01-23	2011-02-08	2011-02-28	2011-03-20	2011-04-11
MJD	55574	55584	55600	55620	55640	55662
Model: wabs*cutoffpl						
Parameter	Obs#1	Obs#2	Obs#3	Obs#4	Obs#5	Obs#6
N_H [10^{21} cm $^{-2}$]	$0.63^{+0.06}_{-0.06}$	$0.63^{+0.06}_{-0.06}$	$0.65^{+0.08}_{-0.08}$	$0.65^{+0.10}_{-0.10}$	$0.34^{+0.12}_{-0.12}$	$0.39^{+0.12}_{-0.12}$
Γ	$0.45^{+0.03}_{-0.03}$	$0.88^{+0.03}_{-0.03}$	$0.91^{+0.04}_{-0.04}$	$0.81^{+0.04}_{-0.04}$	$0.54^{+0.05}_{-0.05}$	$0.85^{+0.05}_{-0.05}$
E_{cut} [keV]	$1.56^{+0.02}_{-0.02}$	$2.19^{+0.03}_{-0.03}$	$3.03^{+0.06}_{-0.06}$	$3.51^{+0.09}_{-0.09}$	$3.23^{+0.09}_{-0.09}$	$4.52^{+0.17}_{-0.16}$
$f_{\text{PCA/XRT}}$	$0.89^{+0.01}_{-0.01}$	$1.06^{+0.01}_{-0.01}$	$1.11^{+0.02}_{-0.02}$	$1.07^{+0.02}_{-0.02}$	$1.12^{+0.02}_{-0.02}$	$1.02^{+0.02}_{-0.02}$
F_{CPL}	4.01	2.91	2.10	1.74	1.30	0.98
χ^2_ν (d.o.f.)	1.32 (426)	1.26 (389)	1.17 (316)	1.04 (309)	0.94 (251)	1.10 (187)
Model: wabs*(diskBB+BB)						
Parameter	Obs#1	Obs#2	Obs#3	Obs#4	Obs#5	Obs#6
N_H [10^{21} cm $^{-2}$]	$0.54^{+0.04}_{-0.04}$	$0.28^{+0.05}_{-0.05}$	$0.21^{+0.06}_{-0.06}$	$0.24^{+0.06}_{-0.06}$	$0.24^{+0.07}_{-0.08}$	$0.00^{+0.06}_{-0.06}$
kT_{in} [keV]	$0.96^{+0.02}_{-0.02}$	$0.80^{+0.02}_{-0.02}$	$0.99^{+0.03}_{-0.03}$	$1.30^{+0.06}_{-0.05}$	$1.69^{+0.11}_{-0.10}$	$1.37^{+0.03}_{-0.06}$
$R_{\text{in}}\sqrt{\cos i}$ [km]	$13.9^{+0.6}_{-0.5}$	$14.9^{+0.6}_{-0.6}$	$7.9^{+0.4}_{-0.4}$	$4.4^{+0.3}_{-0.3}$	$2.5^{+0.2}_{-0.2}$	$2.7^{+0.2}_{-0.2}$
kT_{BB} [keV]	$1.32^{+0.05}_{-0.05}$	$1.25^{+0.02}_{-0.02}$	$1.61^{+0.03}_{-0.03}$	$2.03^{+0.07}_{-0.06}$	$2.49^{+0.36}_{-0.22}$	$2.25^{+0.09}_{-0.07}$
$R_{\text{BB},10\text{kpc}}$ [km]	$3.7^{+0.6}_{-0.6}$	$5.5^{+0.3}_{-0.3}$	$3.0^{+0.2}_{-0.2}$	$1.7^{+0.2}_{-0.2}$	$0.8^{+0.3}_{-0.3}$	$1.2^{+0.1}_{-0.1}$
$f_{\text{PCA/XRT}}$	$0.89^{+0.01}_{-0.01}$	$1.07^{+0.01}_{-0.01}$	$1.11^{+0.02}_{-0.02}$	$1.05^{+0.02}_{-0.02}$	$1.11^{+0.02}_{-0.02}$	$1.01^{+0.02}_{-0.02}$
F_{diskBB}	3.54	1.87	1.30	1.16	1.05	0.57
F_{BB}	0.44	0.79	0.63	0.51	0.26	0.37
χ^2_ν (d.o.f.)	1.25 (425)	1.54 (388)	1.46 (315)	1.15 (308)	0.90 (250)	1.31 (186)
Model: wabs*(BB+nthcomp)						
Parameter	Obs#1	Obs#2	Obs#3	Obs#4	Obs#5	Obs#6
N_H [10^{21} cm $^{-2}$]	$0.00^{+0.17}_{-0.17}$	$0.00^{+0.08}_{-0.08}$	$0.00^{+0.09}_{-0.09}$	$0.00^{+0.21}_{-0.21}$	$0.00^{+0.11}_{-0.11}$	$0.00^{+0.55}_{-0.55}$
kT_{BB} [keV]	$0.28^{+0.01}_{-0.01}$	$0.28^{+0.01}_{-0.01}$	$0.29^{+0.01}_{-0.01}$	$0.29^{+0.01}_{-0.02}$	$0.28^{+0.02}_{-0.02}$	$0.27^{+0.02}_{-0.02}$
R_{BB} [km]	98^{+18}_{-3}	95^{+7}_{-3}	67^{+5}_{-3}	52^{+10}_{-3}	43^{+5}_{-3}	43^{+25}_{-3}
Γ	$2.98^{+0.23}_{-0.18}$	$2.51^{+0.16}_{-0.16}$	$2.26^{+0.07}_{-0.10}$	$2.17^{+0.09}_{-0.08}$	$2.17^{+0.16}_{-0.12}$	$1.98^{+0.09}_{-0.07}$
kT_e [keV]	$1.52^{+0.12}_{-0.09}$	$1.63^{+0.12}_{-0.13}$	$2.07^{+0.13}_{-0.06}$	$2.50^{+0.17}_{-0.13}$	$2.57^{+0.29}_{-0.19}$	$2.79^{+0.22}_{-0.16}$
kT_{seed} [keV]	$0.58^{+0.03}_{-0.03}$	$0.60^{+0.04}_{-0.05}$	$0.64^{+0.05}_{-0.02}$	$0.67^{+0.05}_{-0.05}$	$0.73^{+0.06}_{-0.09}$	$0.67^{+0.06}_{-0.09}$
τ	$8.7^{+1.0}_{-1.1}$	$10.3^{+1.4}_{-1.1}$	$10.3^{+0.8}_{-0.8}$	$9.8^{+0.8}_{-0.8}$	$9.7^{+1.2}_{-1.4}$	$10.5^{+0.9}_{-1.0}$
R_{seed} [km]	44^{+3}_{-3}	32^{+4}_{-3}	24^{+1}_{-3}	21^{+3}_{-2}	16^{+3}_{-2}	15^{+4}_{-2}
$f_{\text{PCA/XRT}}$	$0.88^{+0.01}_{-0.01}$	$1.03^{+0.01}_{-0.01}$	$1.09^{+0.02}_{-0.02}$	$1.04^{+0.02}_{-0.02}$	$1.10^{+0.02}_{-0.02}$	$1.00^{+0.02}_{-0.02}$
F_{BB}	1.16	1.14	0.66	0.38	0.24	0.20
F_{nthcomp}	2.92	1.85	1.48	1.40	1.14	0.81
χ^2_ν (d.o.f.)	1.19 (423)	1.14 (386)	1.10 (313)	1.00 (306)	0.89 (248)	1.02 (184)
Model: wabs*(diskBB+nthcomp)						
Parameter	Obs#1	Obs#2	Obs#3	Obs#4	Obs#5	Obs#6
N_H [10^{21} cm $^{-2}$]	$0.93^{+0.16}_{-0.15}$	$0.79^{+0.11}_{-0.11}$	$0.76^{+0.16}_{-0.15}$	$0.85^{+0.23}_{-0.23}$	$0.53^{+0.24}_{-0.22}$	$0.89^{+0.35}_{-0.32}$
kT_{in} [keV]	$0.34^{+0.03}_{-0.03}$	$0.42^{+0.03}_{-0.03}$	$0.45^{+0.05}_{-0.04}$	$0.40^{+0.07}_{-0.05}$	$0.50^{+0.12}_{-0.08}$	$0.37^{+0.07}_{-0.05}$
$R_{\text{in}}\sqrt{\cos i}$ [km]	71^{+16}_{-13}	44^{+7}_{-6}	29^{+7}_{-6}	27^{+9}_{-7}	14^{+6}_{-5}	24^{+11}_{-8}
Γ	$2.75^{+0.04}_{-0.03}$	$2.72^{+0.05}_{-0.05}$	$2.33^{+0.04}_{-0.04}$	$2.19^{+0.03}_{-0.03}$	$2.31^{+0.06}_{-0.05}$	$2.02^{+0.03}_{-0.03}$
kT_e [keV]	$1.41^{+0.10}_{-0.07}$	$1.72^{+0.19}_{-0.13}$	$2.12^{+0.15}_{-0.12}$	$2.51^{+0.19}_{-0.15}$	$2.76^{+0.43}_{-0.27}$	$2.88^{+0.28}_{-0.20}$
kT_{seed} [keV]	$0.55^{+0.02}_{-0.02}$	$0.67^{+0.03}_{-0.03}$	$0.70^{+0.05}_{-0.04}$	$0.69^{+0.05}_{-0.04}$	$0.82^{+0.07}_{-0.05}$	$0.71^{+0.06}_{-0.05}$
τ	$10.0^{+0.5}_{-0.6}$	$9.1^{+0.6}_{-0.7}$	$9.8^{+0.5}_{-0.6}$	$9.7^{+0.5}_{-0.6}$	$8.5^{+0.8}_{-1.0}$	$10.0^{+0.6}_{-0.7}$
R_{seed} [km]	51^{+2}_{-2}	25^{+2}_{-2}	20^{+2}_{-2}	20^{+2}_{-2}	13^{+1}_{-2}	14^{+2}_{-1}
$f_{\text{PCA/XRT}}$	$0.88^{+0.01}_{-0.01}$	$1.03^{+0.01}_{-0.01}$	$1.10^{+0.02}_{-0.02}$	$1.05^{+0.02}_{-0.02}$	$1.10^{+0.02}_{-0.02}$	$1.00^{+0.02}_{-0.02}$
F_{diskBB}	1.32	1.25	0.70	0.41	0.26	0.23
F_{nthcomp}	3.02	1.71	1.40	1.38	1.09	0.81
χ^2_ν (d.o.f.)	1.19 (423)	1.09 (386)	1.10 (313)	1.00 (306)	0.88 (248)	1.01 (184)

- (i) All errors represent the 90% confidence limits of statistical uncertainty for a single parameter of interest.
- (ii) R_{BB} is a BB-model parameter representing the source radius if the source distance is 10 kpc.
- (iii) $R_{\text{in}}\sqrt{\cos i}$ is a diskBB-model parameter related to the inner radius of the accretion disk R_{in} and the disk inclination i in the assumed 10 kpc source distance.
- (iv) R_{seed} is a radius of blackbody seed photons in the thermally Comptonized continuum model (nthcomp) in the assumed 10 kpc source distance.
- (v) F_{CPL} , F_{BB} , F_{diskBB} , F_{nthcomp} represent absorption-corrected fluxes of each continuum model of cutoffpl, BB, diskbb, and nthcomp, respectively, in units of 10^{-9} erg cm $^{-2}$ s $^{-1}$ in 0.1-100 keV band.

tailed model parameters differ significantly between the two states). The obtained E_{cut} of 1.5–5 keV seems to be too high as the temperature for the accretion disk in BH binaries, which is typically below 1 keV, and is also too low for the cutoff energy of the Comptonized component, which is usually higher than 50 keV (e.g. McClintock & Remillard 2006). However, the peculiar Galactic BH binary, GRS 1915+105, sometimes shows in the bright phases such a spectrum as represented by `diskBB` with $kT_{\text{in}} \sim 2$ keV (Done et al. 2004). Therefore, the possibility of a BH X-ray binary cannot be completely ruled out from the spectral parameters alone. As has been seen in the CDs and HIDs (section 3.2), the spectral time evolution, to be explored below, gives us another helpful information to identify the source nature.

4.2. Emission Geometry in NS-LMXB Scenario

According to the widely accepted picture of NS-LMXBs (e.g. Mitsuda et al. 1984, Mitsuda et al. 1989), the two continuum components in the `wabs*(diskBB+nthcomp)` model are interpreted as a thermal emission from the accretion disk (`diskBB`), and a blackbody emission from the NS surface (the boundary layer) modified through Comptonization by surrounding hot electrons (`nthcomp`). In figure 7b, time evolution of the parameters of these physical components are plotted.

In order for the `diskBB` model to be physical, its inner disk radius has to be larger than the NS radius, ~ 10 km. We may derive a realistic estimate of the inner disk radius, r_{in} , from the model parameter $R_{\text{in}}\sqrt{\cos i}$ as

$$r_{\text{in}} = \xi \kappa^2 R_{\text{in}} \\ = 1.2 \left(\frac{\xi}{0.41} \right) \left(\frac{\kappa}{1.7} \right)^2 \left(\frac{d_{10}}{\sqrt{\cos i}} \right) \cdot R_{\text{in}} \sqrt{\cos i}, \quad (3)$$

where $\xi = 0.41$ is a correction factor for the inner boundary condition (Kubota et al. 1998; Makishima et al. 2000), $\kappa = 1.7$ is the standard color hardening factor (Shimura & Takahara 1995), and d_{10} is the source distance in units of 10 kpc. Here we adopted the same canonical ξ and κ values as for the accretion disk around a black hole. We find that r_{in} changed from $\sim 80 (d_{10}/\sqrt{\cos i})$ km to $\sim 20 (d_{10}/\sqrt{\cos i})$ km across the observations.

If the source distance is > 17 kpc as estimated in section 4.1, the condition of $r_{\text{in}} > 10$ km is always satisfied. The best-fit parameters also satisfy the expected relations of $R_{\text{seed}} < r_{\text{in}}$ and $kT_{\text{seed}} > kT_{\text{in}}$. Thus, the derived model parameters are reasonable, although the range of $kT_{\text{in}} \sim 0.3 - 0.6$ keV seems to be slightly lower than the typical values as obtained in Cyg X-2 (Di Salvo et al. 2002), Aql X-1 (Sakurai et al. 2012), and 4U 1705-44 (Lin et al. 2010) from the BeppoSAX or Suzaku X-ray spectra covering the 0.2–50 keV band.

The seed photons of the Comptonized emission in the `nthcomp` component are considered to mainly originate from a region near the NS surface, to be called the boundary layer. The obtained temperatures of $kT_{\text{seed}} \approx 0.7$ keV and $kT_e \approx 1.5 - 3$ keV, agree with those of NS LMXBs (either Z sources or atoll sources) in the soft state, derived

using the same spectral model (e.g. Gierliński & Done 2002b; Farinelli et al. 2005; Raichur et al. 2011; Sakurai et al. 2012). As seen in figure 7b, however, the estimated radius of the BB seed photons sphere, R_{seed} , changed from $\sim 40 d_{10}$ km to $\sim 10 d_{10}$ km. If the source distance is > 17 kpc as estimated in section 4.1, R_{seed} becomes significantly larger than the typical NS radius of ~ 10 km. This could be explained if the emission from the accretion disk also contributed to the seed photons.

As shown so far, the combination of a disk emission and a Comptonized blackbody component can consistently explain the spectral parameters of MAXI J0556–332. Figure 8 illustrates a possible source geometry implied by the model. The relatively low values of kT_{in} may be explained by the suggested obscuration of the innermost disk region by the Compton corona.

4.3. Long-Term Spectral Evolution

Over the initial ~ 70 days, figure 7b reveals a decrease in both r_{in} and R_{seed} , and increase in kT_e . These changes are considered to reflect the evolution in the X-ray emission region as illustrated in figure 8.

Gilfanov et al. (2003) and Revnivtsev & Gilfanov (2006) reported that the spectrum of the boundary layer at the NS surface can be approximated by a saturated ($\tau \gg 1$) Comptonization model with $kT_e \approx 2 - 4$ keV, to which our results agree. Popham & Sunyaev (2001) numerically explored the same issue, and suggested that the boundary layer would expand at luminosities near L_{EDD} . In such a condition, the optical depth of the Comptonization media would be further increased. The observed relations between the flux and spectrum agree with the expected tendency, although more detailed quantitative study is out of the scope of this paper.

4.4. State Transition in Color-Color Diagram

State transitions are considered to reflect changes of the physical condition in the emission region including the NS surface (or the boundary layer) and the accretion disk, mainly in response to changes in the luminosity. On the basis of the Z source features seen in the CD/HID tracks extracted from the RXTE/PCA data, Homan et al. (2011) reported that MAXI J0556–322 is the third transient Z source after XTE J1701–462 (Homan et al. 2010) and IGR J17480–2446 (Altamirano et al. 2010). They also reported on a source transition between the two types of Z source tracks, from Cyg-like to Sco-like substates. This kind of transition has been observed previously only from XTE J1701–462, which exhibited all three kinds of the CD/HID tracks (Cyg-like Z, Sco-like Z, and atoll) during the decay phase of its outburst in 2006–2007 (Homan et al. 2010). Actually, in figure 3 and figure 4, we confirmed that these tracks are classified into either Cyg-like Z (int-A, B, C, and E) or Sco-like Z (int-D and F). These CDs and HIDs resemble those of XTE J1701–462 in the 2006–2007 outburst (Homan et al. 2007).

The other two transient Z sources, XTE J1701–462 and IGR J17480–2446, showed type-I X-ray bursts (Lin et al. 2009; Chakraborty & Bhattacharyya 2011). However, we

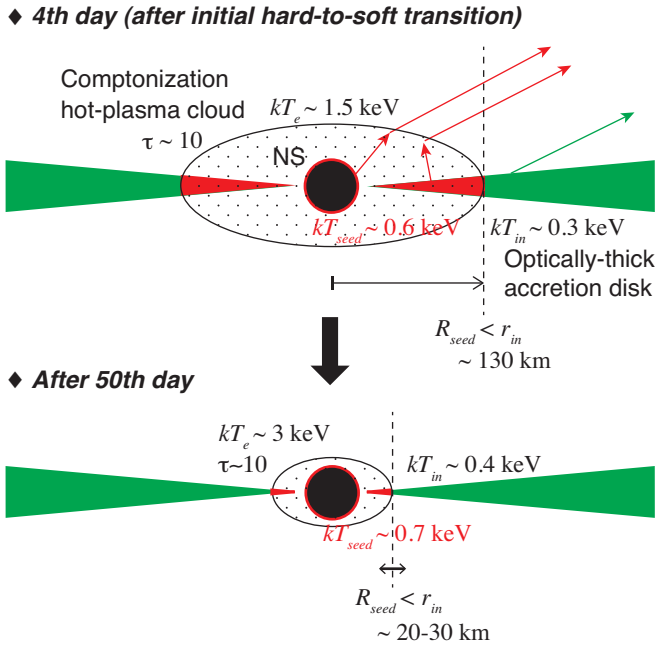


Fig. 8. A schematic view of X-ray emission region including the NS surface, the accretion disk, and the surrounding hot-plasma cloud, implied by the best-fit spectral model on the fourth day (top panel) and after 50th day (bottom panel) from the activity onset. A source distance of 26 kpc is employed to calculate R_{seed} and r_{in} .

did not find any burst-like events.

4.5. Distance Estimate and Source Location

Homan et al. (2011) estimated the distance of MAXI J0556–322 to be 20–35 kpc assuming that the transition between the Cyg-like and the Sco-like substates occurred at the same luminosity as that in XTE J1701–462, whose distance is estimated to be 8.8 kpc from the luminosity of its type-I X-ray bursts (Lin et al. 2009). In the energy-sorted light curves in figure 2, the substate transition occurred when the 2.0–3.6 keV PCA count rate crossed ~ 14 c s $^{-1}$. For comparison, XTE J1701–462 exhibited the transition at the PCA count rate of ~ 80 c s $^{-1}$ in 2.0–2.9 keV, or 121 c s $^{-1}$ in the 2.0–3.6 keV. Assuming that the two sources make the transition at the same intrinsic luminosity, MAXI J0556–322 is then estimated to be 2.9 times farther, located at $d \sim 26$ kpc; this reconfirms the estimate by Homan et al. (2011). This estimate and the Galactic coordinates of $(l, b) = (238^\circ.9, -25^\circ.2)$ indicate its location of 11 kpc below the Galactic plane and 31 kpc away from the Galactic center. This places the source on outskirts of the Galactic halo, where the population of LMXBs is rather small (Grimm et al. 2002).

Assuming $d = 26$ kpc, the observed maximum flux of 4.3×10^{-9} erg cm $^{-2}$ s $^{-1}$ in the initial phase can be converted to the absorption-corrected luminosity of 3.5×10^{38} erg s $^{-1}$. This is twice as high as the Eddington limit for the typical $1.4 M_\odot$ NS, and agrees with the maximum luminosity in some bright NS LMXBs such as Sco X-1 (D’Aí et al. 2007).

4.6. Initial Transition

The MAXI/GSC light curve in figure 5 reveals a hard-to-soft state transition which occurred on the fourth day from the brightening onset, at the middle of the initial brightening phase. As seen in other transient NS LMXBs (Asai et al. 2012) as well as BH LMXBs (Gierliński & Newton 2006), this transition may be interpreted as the initial formation of an optically-thick accretion disk. The observed X-ray flux just before the transition was 1.0×10^{-9} erg cm $^{-2}$ s $^{-1}$ in the 2–10 keV band.

By comparing the Swift/BAT and the MAXI/GSC data, Asai et al. (2012) investigated outburst rising behavior in the two transient NS binaries, Aql X-1 and 4U 1608–52, and revealed that the initial hard-to-soft state transition of these sources occur at a 2–15 keV luminosity of $0.5 \times 10^{36} - 2 \times 10^{37}$ erg s $^{-1}$. If the distance to MAXI J0556–322 is > 17 kpc as estimated above, the initial hard-to-soft transition is inferred to have occurred at a luminosity of $> 3.5 \times 10^{37}$ erg s $^{-1}$. It is significantly higher than that in Aql X-1 and 4U 1608–52. Further discussion on this point requires more detailed consideration of the inclination angle, and possible differences in magnetic field strengths.

5. Conclusion

Throughout the active period which lasted for more than one year, the 0.5–30 keV X-ray spectra of the new X-ray transient, MAXI J0556–322, obtained by the Swift/XRT and RXTE/PCA were successfully represented by a two-component model, consisting of an optically-thick thermal emission from an accretion disk with an inner-disk temperature of $kT \approx 0.3 - 0.4$ keV, and a Comptonized emission of thermal seed photons of $kT_{\text{seed}} \approx 0.6 - 0.8$ keV by hot electrons with $kT_e \approx 1.5 - 3$ keV. The obtained model parameters are consistent with those of NS LMXBs when their luminosity is higher than $\sim 0.1 L_{\text{EDD}}$. This, together with the source behavior on CDs, constrains the source distance to be > 17 kpc, most likely 26 kpc, and place the source on outskirts of the Galactic halo. The long-term spectral variations can be understood by evolution of the accretion disk and the emission region on the NS. The MAXI/GSC light curve revealed a hard-to-soft transition in the middle of the initial brightening phase. The transition luminosity would be significantly higher than those observed in other typical transient NS LMXBs.

We appreciate all MAXI science and operation team members for their dedicated works to enable the science analysis of MAXI data. We also thank Drs. K. Makishima, K. Asai, and H. Takahashi for their stimulating discussions. This research has made use of RXTE data obtained from the High Energy Astrophysics Science Archive Research Center (HEASARC) provided by NASA/GSFC; and Swift data supplied by the UK Swift Science Data Centre at the University of Leicester. This research work is partially supported by the Ministry

of Education, Culture, Sports, Science and Technology (MEXT), Grant-in-Aid for Science Research 20244015.

References

- Altamirano, D., Homan, J., Linares, M., et al. 2010, *The Astronomer's Telegram*, 2952, 1
- Asai, K., Matsuoka, M., Mihara, T., et al. 2012, arXiv:1206.3927
- Barret, D., Olive, J. F., Boirin, L., et al. 2000, *ApJ*, 533, 329
- Barret, D., & Olive, J.-F. 2002, *ApJ*, 576, 391
- Belloni, T., Motta, S., Munoz-Darias, T., & Stiele, H. 2011, *The Astronomer's Telegram*, 3112, 1
- Burrows, D. N., Hill, J. E., Nousek, J. A., et al. 2005, *Space Sci. Rev.*, 120, 165
- Chakraborty, M., & Bhattacharyya, S. 2011, *ApJL*, 730, L23
- Church, M. J., & Balucińska-Church, M. 2001, *A&A*, 369, 915
- Coriat, M., Tzioumis, T., Corbel, S., et al. 2011, *The Astronomer's Telegram*, 3119, 1
- Cornelisse, R., D'Avanzo, P., Campana, S., et al. 2011, arXiv:1111.6946
- D'Aí, A., Życki, P., Di Salvo, T., et al. 2007, *ApJ*, 667, 411
- Di Salvo, T., Robba, N. R., Iaria, R., et al. 2001, *ApJ*, 554, 49
- Di Salvo, T., Farinelli, R., Burderi, L., et al. 2002, *A&A*, 386, 535
- Done, C., Wardziński, G., & Gierliński, M. 2004, *MNRAS*, 349, 393
- Falanga, M., Belloni, T., & Campana, S. 2006, *A&A*, 456, L5
- Farinelli, R., Frontera, F., Zdziarski, A. A., et al. 2005, *A&A*, 434, 25
- Gehrels, N., Chincarini, G., Giommi, P., et al. 2004, *ApJ*, 611, 1005
- Gierliński, M., & Done, C. 2002, *MNRAS*, 331, L47
- Gierliński, M., & Done, C. 2002, *MNRAS*, 337, 1373
- Gierliński, M., & Newton, J. 2006, *MNRAS*, 370, 837
- Gilfanov, M., Revnivtsev, M., & Molokov, S. 2003, *A&A*, 410, 217
- Godet, O., Beardmore, A. P., Abbey, A. F., et al. 2009, *A&A*, 494, 775
- Grimm, H.-J., Gilfanov, M., & Sunyaev, R. 2002, *A&A*, 391, 923
- Hasinger, G., & van der Klis, M. 1989, *A&A*, 225, 79
- Jahoda, K., Markwardt, C. B., Radeva, Y., Rots, A. H., Stark, M. J., Swank, J. H., Strohmayer, T. E., & Zhang, W. 2006, *ApJS*, 163, 401
- Halpern, J. P. 2011, *The Astronomer's Telegram*, 3104, 1
- Hayakawa, S. 1981, *Space Sci. Rev.*, 29, 221
- Hiroi, K., Ueda, Y., Isobe, N., et al. 2011, *PASJ*, 63, 677
- Homan, J., van der Klis, M., Wijnands, R., et al. 2007, *ApJ*, 656, 420
- Homan, J., van der Klis, M., Fridriksson, J. K., et al. 2010, *ApJ*, 719, 201
- Homan, J., Linares, M., van den Berg, M., & Fridriksson, J. 2011, *The Astronomer's Telegram*, 3650, 1
- Kalberla, P. M. W., Burton, W. B., Hartmann, D., et al. 2005, *A&A*, 440, 775
- Kennea, J. A., Evans, P. A., Krimm, H., et al. 2011, *The Astronomer's Telegram*, 3103, 1
- Kubota, A., Tanaka, Y., Makishima, K., et al. 1998, *PASJ*, 50, 667
- Lewin, W. H. G., van Paradijs, J., & Taam, R. E. 1993, *Space Sci. Rev.*, 62, 223
- Lin, D., Remillard, R. A., & Homan, J. 2007, *ApJ*, 667, 1073
- Lin, D., Remillard, R. A., & Homan, J. 2009, *ApJ*, 696, 1257
- Lin, D., Altamirano, D., Homan, J., et al. 2009, *ApJ*, 699, 60
- Lin, D., Remillard, R. A., & Homan, J. 2010, *ApJ*, 719, 1350
- Makishima, K., Maejima, Y., Mitsuda, K., et al. 1986, *ApJ*, 308, 635
- Makishima, K., Kubota, A., Mizuno, T., et al. 2000, *ApJ*, 535, 632
- Maitra, D., Miller, J. M., Raymond, J. C., & Reynolds, M. T. 2011, *ApJL*, 743, L11
- Matsumura, T., Negoro, H., Suwa, F., et al. 2011, *The Astronomer's Telegram*, 3102, 1
- Matsuoka, M., et al. 2009, *PASJ*, 61, 999
- McClintock, J. E., & Remillard, R. A. 2006, *Compact stellar X-ray sources*, 157
- Mihara, T., Nakajima, M., Sugizaki, et al. 2011, *PASJ*, 63, 623
- Mitsuda, K., Inoue, H., Koyama, K., et al. 1984, *PASJ*, 36, 741
- Mitsuda, K., Inoue, H., Nakamura, N., & Tanaka, Y. 1989, *PASJ*, 41, 97
- Morrison, R., & McCammon, D. 1983, *ApJ*, 270, 119
- Nakahira, S., et al. 2010, *PASJ*, 62, L27
- Paizis, A., Farinelli, R., Titarchuk, L., et al. 2006, *A&A*, 459, 187
- Popham, R., & Sunyaev, R. 2001, *ApJ*, 547, 355
- Raichur, H., Misra, R., & Dewangan, G. 2011, *MNRAS*, 416, 637
- Revnivtsev, M. G., & Gilfanov, M. R. 2006, *A&A*, 453, 253
- Rothschild, R. E., Blanco, P. R., Gruber, D. E., et al. 1998, *ApJ*, 496, 538
- Russell, D. M., Lewis, F., Doran, R., & Roberts, S. 2011, *The Astronomer's Telegram*, 3116, 1
- Sakurai, S., Yamada, S., Torii, S., et al. 2012, arXiv:1201.5891
- Shakura, N. I., & Sunyaev, R. A. 1973, *A&A*, 24, 337
- Shimura, T., & Takahara, F. 1995, *ApJ*, 445, 780
- Singh, K. P., & Apparao, K. M. V. 1994, *ApJ*, 431, 826
- Sriram, K., Rao, A. R., & Choi, C. S. 2011, *ApJL*, 743, L31
- Strohmayer, T. E., & Smith, E. A. 2011, *The Astronomer's Telegram*, 3106, 1
- Strohmayer, T. E. 2011, *The Astronomer's Telegram*, 3110, 1
- Sugizaki, M., Mihara, T., Serino, M., et al. 2011, *PASJ*, 63, 635
- Sunyaev, R. A., & Titarchuk, L. G. 1980, *A&A*, 86, 121
- Takahashi, H., Sakurai, S., & Makishima, K. 2011, *ApJ*, 738, 62
- Tarana, A., Belloni, T., Bazzano, A., Méndez, M., & Ubertini, P. 2011, *MNRAS*, 416, 873
- Tomida, H., Tsunemi, H., Kimura, M., et al. 2011, *PASJ*, 63, 397
- Tsunemi, H., Tomida, H., Katayama, H., et al. 2010, *PASJ*, 62, 1371
- van der Klis, M. 2006, *Compact stellar X-ray sources*, 39
- White, N. E., Stella, L., & Parmar, A. N. 1988, *ApJ*, 324, 363
- Yamaoka, K., Allured, R., Kaaret, P., et al. 2011, arXiv:1110.6512
- Zdziarski, A. A., Johnson, W. N., & Magdziarz, P. 1996, *MNRAS*, 283, 193
- Życki, P. T., Done, C., & Smith, D. A. 1999, *MNRAS*, 309, 561